European Journal of Radiology Open 11 (2023) 100500

Contents lists available at ScienceDirect

European Journal of Radiology Open

journal homepage: www.elsevier.com/locate/ejro

Original article

Utility of contrast-enhanced 3D STIR FLAIR imaging for evaluating pituitary adenomas at 3 Tesla

Iichiro Osawa *, Keita Nagawa, Yuki Hara, Hirokazu Shimizu, Sayuri Tanaka, Eito Kozawa

Department of Radiology, Saitama Medical University Hospital, 38 Morohongo, Moroyama-machi, Iruma-gun, Saitama 350-0495, Japan

ARTICLE INFO

Keywords:
Pituitary adenoma
Pituitary gland
3D STIR FLAIR
T1-weighted imaging
Magnetic resonance imaging

ABSTRACT

Purpose: To assess the usefulness of contrast-enhanced 3D STIR FLAIR imaging for evaluation of pituitary adenomas.

Methods: Patients with pituitary adenomas underwent MR examinations including contrast-enhanced 3D STIR FLAIR and 2D T1-weighted (T1W) imaging. We subjectively compared the two techniques in terms of 10 categories. In addition, images were rated by side-by-side comparisons into three outcomes: 3D STIR FLAIR imaging superior, equal, or 2D T1W imaging superior. Additionally, the added value of 3D STIR FLAIR imaging for adenoma detection over conventional MR imaging was assessed.

Results: Twenty-one patients were included in this study. 3D STIR FLAIR imaging offered significantly better images than 2D T1W imaging in terms of three categories, including overall visualization of the cranial nerves in the cavernous sinus (mean 4.0 vs. 2.8, $p < 0.0001$), visualization of the optic nerves and chiasm (mean 4.0 vs. 2.6, $p < 0.0001$), and severity of susceptibility artifacts (mean 0.0 vs. 0.4, $p = 0.004$). In the side-by-side comparison, 3D STIR FLAIR imaging was judged to be significantly superior to 2D T1W imaging for overall lesion conspicuity (62% vs. 19%, $p = 0.049$) and border between the adenoma and the pituitary gland (67% vs. 19%, $p = 0.031$). The addition of 3D STIR FLAIR imaging significantly improved the adenoma detection of conventional MR imaging.

Conclusion: 3D STIR FLAIR imaging improved overall lesion conspicuity compared to 2D T1W imaging. We suggest that 3D STIR FLAIR imaging is recommended as a supplemental technique when pituitary adenomas are invisible or equivocal on conventional imaging.

1. Introduction

MR imaging has emerged as the modality of choice for standard diagnostic imaging of pituitary adenomas, which requires high spatial and contrast resolution. Contrast-enhanced T1-weighted (T1W) imaging, including conventional and dynamic imaging, plays an important role in the evaluation of pituitary adenomas and surrounding structures. Conventional 2D spin echo (SE) T1W imaging is commonly used as non-dynamic contrast-enhanced imaging, while dynamic imaging can visualize pituitary adenomas that are not visible on conventional T1W imaging [1]. Despite advancements in dynamic imaging, this technique has several drawbacks. Even with dynamic imaging, small microadenomas can be easily missed due to the tumor size and limited spatial resolution of the MR scanner [2]. Another disadvantage is the relatively low contrast between the tumor and the normal pituitary gland [2]. Additionally, the border between adenoma and normal pituitary gland in some cases may be ill-defined, which can make it difficult to detect microadenomas.

3D gradient echo (GRE) T1W imaging has been an alternative, providing improved spatial resolution and soft tissue contrast [3,4]. 3D GRE sequences yield isotropic volume data and thinner section images in arbitrary directions. However, these sequences have two main disadvantages: susceptibility artifacts and high signal in vessels. Susceptibility artifacts are usually observed at the interface between the sella and sphenoid sinus, which may mimic or obscure pituitary lesions. A high signal in vessels, caused by a short TE, is seen in the cavernous sinus

Abbreviations: T1W, T1-weighted; SE, spin echo; GRE, gradient echo; TSE, turbo spin echo; CSF, cerebrospinal fluid; T2W, T2-weighted; SNR, signal-to-noise ratio; CNR, contrast-to-noise ratio; SIR, signal intensity ratio; ROI, region of interest; SI, signal intensity; SD, standard deviation; CI, confidence interval; BBB, blood-brain barrier; MIP, maximum intensity projection; MPR, multiplanar reconstruction.

* Correspondence to: 38 Morohongo, Moroyama-machi, Iruma-gun, Saitama 350-0495, Japan.
E-mail address: oyabun@saitama-med.ac.jp (I. Osawa).

https://doi.org/10.1016/j.ejro.2023.100500
Received 27 May 2023; Accepted 19 June 2023

and internal carotid artery. This can make it difficult to accurately interpret enhanced lesions within the cavernous sinus [5].

Currently, 3D turbo spin echo (TSE) with variable flip angles is an emerging technique for the evaluation of pituitary lesions [5–7]. This sequence has the potential to provide isotropic thin sections and reduce susceptibility artifacts [6,7]. 3D STIR FLAIR imaging is a type of 3D TSE inversion recovery imaging that uses two different inversion pulses to suppress fat as well as cerebrospinal fluid (CSF). Although 2D STIR FLAIR imaging was used for the evaluation of optic neuritis [8], 3D STIR FLAIR imaging, to the best of our knowledge, has not been used for the evaluation of pituitary adenomas. We aimed to assess the usefulness of contrast-enhanced 3D STIR FLAIR imaging for evaluating pituitary adenomas.

2. Materials and methods

2.1. Patients

We reviewed 78 consecutive patients with clinically suspected pituitary lesions who underwent MR imaging between June 2020 and July 2021. We included patients diagnosed with pituitary adenomas. Patients were excluded if the image quality was insufficient for image interpretation. The present study was approved by the Institutional Review Board of our institution. We obtained written informed consent for the procedures and opt-out consent for the use of retrospective clinical data from all patients.

2.2. MR imaging

MR examination was performed in all patients using a 3 Tesla scanner (Elition, Philips Medical Systems, Best, The Netherlands) with a 32-channel head coil. The MR examination consisted of the following imaging: non-enhanced conventional 2D T2-weighted (T2W) and T1W imaging in the coronal plane, enhanced conventional 2D T1W imaging (performed initially in the coronal plane, followed by the sagittal plane), and pre- and post-contrast 3D STIR FLAIR imaging. After pre-contrast 3D STIR FLAIR imaging, enhanced conventional 2D T1W (coronal and sagittal) imaging and post-contrast 3D STIR FLAIR imaging were performed, where we alternated the order of the two sequences by rotation to avoid timing bias after contrast injection. Table 1 describes the parameters of the 3D STIR FLAIR and the conventional coronal 2D T1W imaging. Sagittal 2D T1W imaging was acquired using the same parameters as coronal 2D T1W imaging, except for the acquisition plane.

Table 1
Parameters of 3D STIR FLAIR and 2D T1W imaging.

	3D STIR FLAIR imaging	Conventional 2D T1W imaging
Acquisition plane	Coronal	Coronal
Fat suppression	STIR	SPIR
TR/TE (ms)	6000/425	477/10
TI (ms)	250/2450	-
Variable flip angle (°)	Min 10, Mid 100, Max 100	-
Flip angle (°)	-	90
TSE factor	80	5
Matrix size	200 × 200	268 × 227
FOV (mm^2)	180 × 180	180 × 180
Acquisition voxel size (mm^2)	0.9 × 0.9	0.7 × 0.8
Reconstruction voxel size (mm^2)	0.4 × 0.4	0.4 × 0.4
Slice thickness, gap (mm)	0.9, − 0.45	3, 0.3
Number of slices	120	15
Bandwidth (Hz/pixel)	932	393
Compressed SENSE factor	4.5	1
Number of excitations	1	2
Acquisition time (min:s)	4:42	2:28

Post-contrast imaging was started at approximately 2 min 30 s after intravenous injection of gadolinium-HP-DO3A (Gadoteridol) at a single 0.2 mL/kg (0.1 mmol/kg) dose.

2.3. Imaging analysis

We conducted both subjective and objective analyses of 3D STIR FLAIR and 2D T1W imaging. For the subjective analyses, all images were reviewed independently by two board-certified radiologists (I. O. and K. N.) who were blinded to the clinical information in random order. Any discrepancies between the readers were resolved through discussion until a consensus was reached. MR imaging review was performed in two sessions.

In the first session, we conducted subjective analysis by comparing the following 10 categories between post-contrast 3D STIR FLAIR and conventional coronal 2D T1W imaging, partially adapted from Kakite et al. [4]: 1) overall lesion conspicuity; 2) border between the adenoma and pituitary gland; 3) border between the adenoma and cavernous sinus; 4) border between the pituitary gland and cavernous sinus; 5) visualization of the pituitary stalk; 6) overall visualization of the cranial nerves in the cavernous sinus; 7) visualization of the optic nerves and chiasm; 8) severity of susceptibility artifacts from the interface between the sphenoid sinus and sella; 9) severity of pulsation artifacts from the internal carotid arteries; and 10) severity of CSF flow artifacts in the cistern. Categories 1–7 were graded according to a 5-point scale: 0 = non-diagnostic, 1 = poor, 2 = fair, 3 = good, and 4 = excellent. Categories 8–10 were assessed according to a 3-point scale: 0 = artifacts are absent, 1 = artifacts are present but do not affect image interpretation, and 2 = artifacts are present and affect image interpretation. In addition, the appearance of the cavernous sinus on post-contrast 3D STIR FLAIR imaging was classified by signal intensity (SI) compared with pre-contrast images into three groups: mostly low, mostly high, and mixed (low and high).

In the second session, each reader individually compared post-contrast 3D STIR FLAIR and coronal 2D T1W imaging side-by-side, and divulged their overall preferred sequence for the three categories as follows: overall lesion conspicuity, border between the adenoma and pituitary gland, and border between the adenoma and cavernous sinus. Each category was divided into three outcomes: 3D STIR FLAIR imaging superior, equal, and 2D T1W imaging superior.

Additionally, the added value of post-contrast 3D STIR FLAIR imaging was evaluated for adenoma detection by another board-certified radiologist (Y.H.) over two sessions. In the first session, the experienced radiologist reviewed the conventional MR imaging (non-contrast 2D T2W and T1W imaging plus enhanced coronal 2D T1W imaging) alone, and scored their confidence level regarding whether pituitary adenoma was present using a 5-point scale. The 5-point confidence scale was defined as follows: 0 = definitely no pituitary adenoma, 1 = probably no pituitary adenoma, 2 = equivocal, 3 = probably pituitary adenoma, and 4 = definitely pituitary adenoma. In the second session, the radiologist reviewed post-contrast 3D STIR FLAIR imaging along with conventional MR imaging, and rescored the confidence level using the same 5-point scale.

Objective analysis was performed by measuring the SI ratio (SIR) in predefined regions of interest (ROIs). The ROI analysis was independently conducted by the two board-certified radiologists using the workstation Synapse VINCENT version 5.2 (Fuji Film, Tokyo, Japan), and the quantitative data obtained by the two radiologists were presented as means and standard deviations (SD). We compared the SIR between pre- and post-contrast 3D STIR FLAIR images. A freehand ROI was drawn in the pituitary adenoma (mean 74 mm^2, range 7–441 mm^2), pituitary gland (mean 33 mm^2, range 13–79 mm^2), or pituitary stalk (mean 8 mm^2, range 4–16 mm^2), while an ovoid ROI (20 mm^2) was placed in the temporal while matter. SIR was calculated as follows: $SIR_{Adenoma\text{-}WM} = SI_{Adenoma}/SI_{WM}$, $SIR_{Pit\text{-}WM} = SI_{Pit}/SI_{WM}$, and $SIR_{Pit.Stalk\text{-}WM} = SI_{Pit.Stalk}/SI_{WM}$. $SI_{Adenoma}$, SI_{Pit}, $SI_{Pit.Stalk}$, and SI_{WM} were the mean

SIs of the pituitary adenoma, pituitary gland, pituitary stalk, and white matter, respectively.

2.4. Statistical analysis

For the subjective analysis, the Wilcoxon signed-rank test was used to assess statistical differences between 3D STIR FLAIR and 2D T1W imaging. The differences among confidence level scores for adenoma detection was evaluated using the same statistical test. For the objective analysis, a paired *t*-test was used to assess the statistical differences between pre- and post-contrast 3D STIR FLAIR imaging. Gwet's AC1 and the intraclass correlation coefficient (ICC) (3, 1) were used as indices of inter-reader reliability. Gwet's AC1 was used instead of assessing Cohen's kappa because this method overcomes the limitation of kappa being sensitive to trait prevalence and marginal probability [9]. ICC (3, 1) was estimated using a two-way random effects model of consistency for a single observation. AC1 and ICC values were interpreted according to the following classifications by Landis and Koch [10]: < 0, indicating no agreement; 0–0.20, slight agreement; 0.21–0.40, fair agreement; 0.41–0.60, moderate agreement; 0.61–0.80, substantial agreement; and 0.81–1, almost perfect agreement. Two-tailed p values less than 0.05 were considered statistically significant. All statistical calculations were conducted using the statistical computing language R (version 4.0.5; http//www.r-project.org/).

3. Results

3.1. Patients

Twenty-one patients with pituitary adenomas were included, and none met the exclusion criteria. The patient cohort included 8 men and 13 women, with an average age of 50 years (range, 22–74 years). There were 8 (38%) patients with prolactinoma, 6 (29%) with nonfunctioning adenoma, 4 (19%) with Cushing's disease, and 3 (14%) with acromegaly. Of the 21 cases, 16 (76%) had pituitary microadenoma. Pituitary adenomas were diagnosed radiologically and clinically (n = 14) or histologically (n = 7). Post-contrast imaging was performed in the following order: 3D STIR FLAIR imaging first (n = 9) and 2D T1W imaging first (n = 12).

3.2. Subjective analysis

Table 2 shows the summary results of the scores from the comparison of 10 categories between 3D STIR FLAIR and 2D T1W imaging. Contrast-enhanced 3D STIR FLAIR imaging offered statistically significantly better images than 2D T1W imaging with regard to the following categories: overall visualization of the cranial nerves in the cavernous sinus (Fig. 1), visualization of the optic nerves and chiasm (Figs. 1, 2, and 3), and severity of susceptibility artifacts. In addition, 3D STIR FLAIR imaging had higher scores for overall lesion conspicuity and border between the adenoma and pituitary gland, though these were not statistically significant. The inter-reader reliability was almost perfect for 3D STIR FLAIR imaging (AC1 = 0.88–1.00) and 2D T1W imaging (AC1 = 0.86–1.00).

With regard to cavernous sinus appearance, out of the 21 cases, 17 patients were mostly low, one patient was mostly high, and three patients were mixed (Fig. 4). In the three cases in the mixed group, the medial venous compartments tended to be high and the lateral venous compartments tended to be low (Fig. 4b). Inter-reader reliability was almost perfect (AC1 = 0.84, 95% confidence interval [CI] = 0.62–1.06).

Table 3 shows the summary results for the side-by-side comparisons between 3D STIR FLAIR and 2D T1W imaging. 3D STIR FLAIR imaging was judged to be statistically significantly superior to 2D T1W imaging for overall lesion conspicuity (13/21 [62%] vs. 4/21 [19%], $p = 0.049$) and identifying the border between the adenoma and the pituitary gland (14/21 [67%] vs. 4/21 [19%], $p = 0.031$). In addition, 3D STIR FLAIR imaging, although not statistically significant, was superior for identifying the border between the adenoma and the cavernous sinus (12/21 [57%] vs. 4/21 [19%], $p = 0.077$). Three cases (14%) exhibited donut-like enhancement along the inner margin of the tumor on 3D STIR FLAIR imaging, but not on 2D T1W imaging (Fig. 3). The inter-reader reliability was almost perfect for overall lesion conspicuity (AC1 = 1.00, 95% CI = 1.00–1.00), identifying the border between the adenoma and the pituitary gland (AC1 = 1.00, 95% CI = 1.00–1.00), and identifying the border between the adenoma and the cavernous sinus (AC1 = 0.91, 95% CI = 0.80–1.02).

Table 2
Subjective comparison of 10 categories between 3D STIR FLAIR and 2D T1W imaging (n = 21).

	Scores			AC1 (95% CI)	
	3D STIR FLAIR imaging	2D T1W imaging	*p* value	3D STIR FLAIR imaging	2D T1W imaging
Overall lesion conspicuity	3.2 ± 1.2	2.7 ± 0.6	0.145	0.98 (0.96–1.00)	0.99 (0.97–1.01)
Border between the adenoma and pituitary gland	3.1 ± 1.2	2.5 ± 0.7	0.101	0.98 (0.95–1.01)	0.97 (0.94–1.00)
Border between the adenoma and cavernous sinus	3.2 ± 1.2	3.2 ± 0.9	0.758	0.95 (0.91–0.99)	0.95 (0.89–1.01)
Border between the pituitary gland and cavernous sinus	2.1 ± 1.1	3.3 ± 0.8	0.001	0.88 (0.79–0.97)	0.96 (0.94–0.99)
Visualization of the pituitary stalk	3.9 ± 0.3	3.7 ± 0.7	0.500	1.00 (0.99–1.00)	0.99 (0.98–1.00)
Overall visualization of the cranial nerves in the cavernous sinus	4.0 ± 0.2	2.8 ± 0.5	< 0.0001	0.99 (0.97–1.00)	0.97 (0.94–1.00)
Visualization of the optic nerves and chiasm	4.0 ± 0.2	2.6 ± 0.5	< 0.0001	0.98 (0.97–1.00)	0.86 (0.77–0.95)
Severity of susceptibility artifacts	0.0 ± 0.0	0.4 ± 0.5	0.004	1.00 (1.00–1.00)	0.95 (0.89–1.02)
Severity of pulsation artifacts	0.0 ± 0.0	0.0 ± 0.2	NA	1.00 (1.00–1.00)	1.00 (1.00–1.00)
Severity of CSF flow artifacts	0.0 ± 0.0	0.0 ± 0.0	NA	1.00 (1.00–1.00)	1.00 (1.00–1.00)

The scores represent mean ± standard deviation. NA not applicable, CI confidence interval.

Table 4 summarizes the comparison results of adenoma detection between the first and second session. In the second session where post-contrast 3D STIR FLAIR imaging was added, the confidence level for adenoma detection was statistically significantly higher than that in the first session (3.57 ± 0.58 vs. 2.57 ± 1.00, $p < 0.0002$).

3.3. Objective analysis

Fig. 5 demonstrates the comparison results of SIR between pre- and post-contrast 3D STIR FLAIR imaging. The pituitary adenoma showed no significant difference in SIR between post- and pre-contrast 3D STIR FLAIR imaging (1.40 ± 0.77 vs. 1.34 ± 0.43, $p = 0.686$). On the other hand, the pituitary gland and stalk showed decreased SIR on post-contrast 3D STIR FLAIR imaging than pre-contrast imaging (gland:

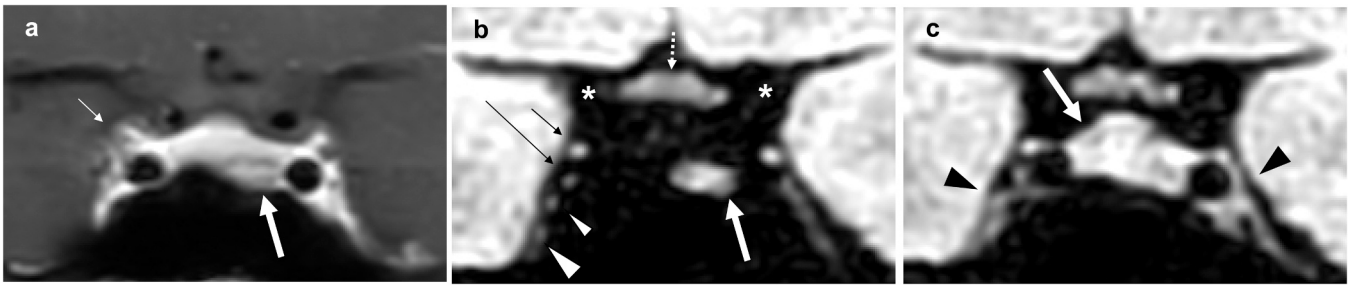

Fig. 1. A 40-year-old woman with pituitary adenoma. Post-contrast 2D T1W imaging (a) shows that the adenoma (arrow) is hypointense compared with the pituitary gland, although the border between the two structures is relatively blurred. The right oculomotor nerve (short arrow) was visible. Post-contrast 3D STIR FLAIR imaging (b) demonstrates that the adenoma (arrow) appears as a hyperintense lesion with a clear border. Cerebrospinal fluid (CSF) flow artifacts are absent within the cisterns (asterisks), and the optic chiasm (dotted arrow) was also more conspicuous than that on 2D T1W imaging. The right oculomotor nerve (short arrow), abducens nerve (long arrow), ophthalmic nerve (small arrowhead), and maxillary nerve (large arrowhead) are more clearly visible than 2D T1W imaging because the signal intensity (SI) of the cavernous sinus is lower than that of pre-contrast imaging (c, arrowheads). Of note, on pre-contrast 3D STIR FLAIR imaging (c), the pituitary gland (arrow) and cavernous sinus (arrowheads) show hyperintensity, and both show decreased signal on corresponding post-contrast imaging (b).

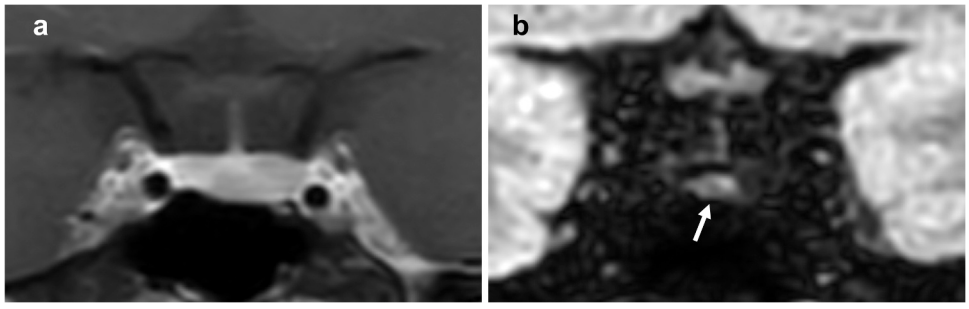

Fig. 2. A 38-year-old woman with pituitary adenoma. On conventional 2D T1W imaging (a), the adenoma is less conspicuous, with the blurred border between the adenoma and pituitary gland. In contrast, post-contrast 3D STIR FLAIR imaging (b) reveals that the adenoma (arrow) is more conspicuous with a sharply demarcated border.

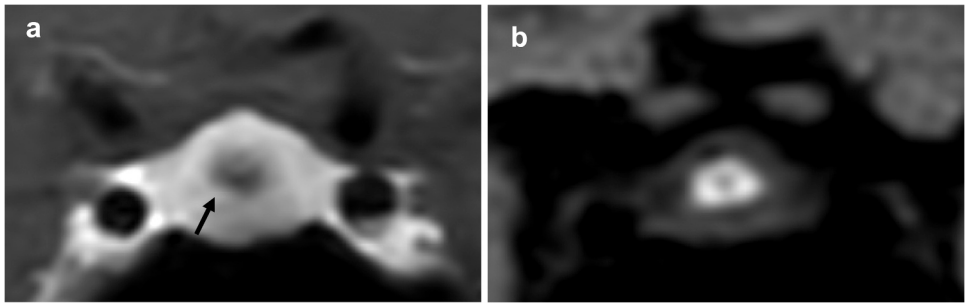

Fig. 3. A 22-year-old woman with pituitary adenoma. Post-contrast 2D T1W imaging (a) showed that the cystic adenoma (arrow) is hypointense without contrast enhancement compared with the pituitary gland, and the border between the two structures is relatively blurred. A thin rim of peripheral enhancement was not observed unlike with reference [27] probably because the normal gland was relatively large compared with the cystic lesion. Post-contrast 3D STIR FLAIR imaging (b) demonstrated that the adenoma appears as a hyperintense lesion and has a clear border. Of note, the adenoma exhibits donut-like enhancement along the inner margin of the cyst.

0.71 ± 0.28 vs. 1.37 ± 0.20, $p < 0.0001$; stalk: 1.14 ± 0.39 vs. 1.39 ± 0.26, $p = 0.012$), although the stalk demonstrated some trends with higher SI compared with the gland. In particular, $SIR_{Pit\text{-}WM}$ was decreased on post-contrast 3D STIR FLAIR imaging in all patients. Inter-reader reliability was almost perfect for $SIR_{Adenoma\text{-}WM}$ (pre-contrast: ICC = 0.91, 95% CI = 0.79–0.96; post-contrast: ICC = 0.91, 95% CI = 0.79–0.96), $SIR_{Pit\text{-}WM}$ (pre-contrast: ICC = 0.88, 95% CI = 0.73–0.95; post-contrast: ICC = 0.98, 95% CI = 0.94–0.99), and $SIR_{Pit.Stalk\text{-}WM}$ (pre-contrast: ICC = 0.88, 95% CI = 0.74–0.95; post-contrast: ICC = 0.96, 95% CI = 0.91–0.99).

4. Discussion

3D STIR FLAIR imaging offered better images than 2D T1W imaging in terms of three categories: overall visualization of the cranial nerves in the cavernous sinus, visualization of the optic nerves and chiasm, and severity of susceptibility artifacts. In addition, 3D STIR FLAIR imaging, although not statistically significant, had higher scores for overall lesion conspicuity and identifying the border between the adenoma and the pituitary gland. In the side-by-side comparison, 3D STIR FLAIR imaging was judged to be superior to 2D T1W imaging for overall lesion conspicuity (62% vs. 19%) and identifying the border between the adenoma and the pituitary gland (67% vs. 19%). In addition, the addition of 3D STIR FLAIR imaging improved adenoma detection over conventional MR imaging.

2D SE T1W imaging, including conventional and dynamic imaging, is most commonly used for the evaluation of pituitary adenomas on post-contrast MR imaging. The normal pituitary gland is intensely enhanced

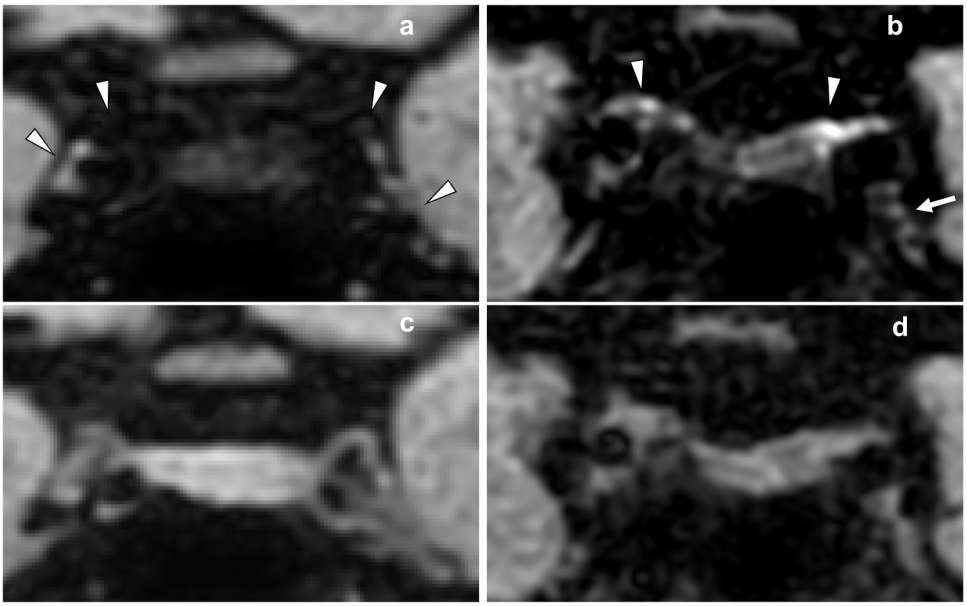

Fig. 4. The cavernous sinus on 3D STIR FLAIR imaging. Post-contrast 3D STIR FLAIR imaging showed that the cavernous sinus exhibits mostly low (a, arrowheads) and mixed (b, arrowheads and arrow) signal intensity (SI) compared with corresponding pre-contrast 3D STIR FLAIR imaging (c and d, respectively). Mixed SI includes hyperintensity in the medial compartment (b, arrowheads) and hypointensity in the other compartments (b, arrow).

Table 3
Subjective comparison between 3D STIR FLAIR and 2D T1W imaging side-by-side (n = 21).

	Overall lesion conspicuity		Border between the adenoma and pituitary gland		Border between the adenoma and cavernous sinus	
	n	%	n	%	n	%
3D STIR FLAIR imaging superior	13	62	14	67	12	57
Equal	4	19	3	14	5	24
2D T1W imaging superior	4	19	4	19	4	19
Total	21	100	21	100	21	100

Table 4
Subjective comparison of adenoma detection between the first and second session (n = 21).

	First session (Conventional MR imaging alone)	Second session (Conventional MR imaging plus post-contrast 3D STIR FLAIR imaging)	
Scale	n	n	
4	4	13	
3	8	7	
2	5	1	
1	4	0	
0	0	0	
Mean scores ± SD	2.57 ± 1.00	3.57 ± 0.58	$p < 0.0002$

SD standard deviation.

on post-contrast T1W imaging due to a lack of the blood-brain barrier (BBB), while pituitary adenoma typically appears as hypointense areas relative to the normal pituitary gland. Moreover, dynamic imaging has emerged as a promising tool for the detection of pituitary adenomas, especially microadenomas. The early phase, during the first 1–2 min after contrast injection, allows for the differentiation between adenoma and normal pituitary tissue [11]. In addition, cystic lesions of the pituitary gland typically exhibit no contrast enhancement on post-contrast T1W imaging [12]. Despite advancements in 2D SE imaging, this technique has several disadvantages. Even with dynamic imaging, small microadenomas can be easily missed due to the tumor size and limited spatial resolution of the MR scanner [2]. Small lesions may be overlooked on MR images using only the coronal direction [13]. Therefore, other alternatives have been explored to overcome these limitations, including T1W imaging using 3D GRE sequences [3,4] and 3D TSE sequences with variable flip angles [6].

STIR sequence is a type of inversion recovery sequence that is usually designed to suppress fat signals by setting an inversion time where the fat signal is null. STIR image illustrates the additive effects of T1 and T2 contrast. This sequence usually cannot be used as a fat suppression technique after gadolinium injection because fat suppression with STIR is not tissue-specific, and gadolinium-containing tissues with a shortened T1 in the fat range can also be suppressed. However, gadolinium-enhanced STIR imaging can provide vascular and background suppression of peripheral nerves, which improves nerve visualization used for MR neurography. In particular, 3D STIR imaging allows higher spatial resolution and isotropic multiplanar reconstruction (MPR) images of arbitrarily reformatted directions, compared with 2D STIR imaging [14–16].

FLAIR sequence is an MR sequence with inversion recovery to a null SI from water. This technique provides greater sensitivity for detecting subtle T1-shortening induced, for example, by contrast material than T1W imaging, and has been applied to various intracranial lesions [17–19]. Pituitary adenomas can be enhanced by post-contrast FLAIR imaging [20]. Several studies have reported that post-contrast 2D FLAIR imaging may be useful in detecting otherwise MRI-negative pituitary microadenomas as foci of hyperintensity [21,22]. In addition, post-contrast 2D FLAIR imaging can provide better tissue contrast for stereotactic radiosurgery planning for pituitary tumors [23]. However, some pituitary adenomas do not show contrast enhancement on FLAIR imaging [22]. 3D FLAIR imaging offers higher spatial resolution and fewer CSF flow and pulsation artifacts than 2D FLAIR imaging [24,25]. The 3D sequence allows the reconstruction of image data using various techniques, including maximum intensity projection (MIP) and MPR [18,26]. One recent report suggested that contrast-enhanced 3D FLAIR imaging can be utilized to differentiate Rathke cleft cysts from cystic pituitary adenomas because the two lesions demonstrated different wall

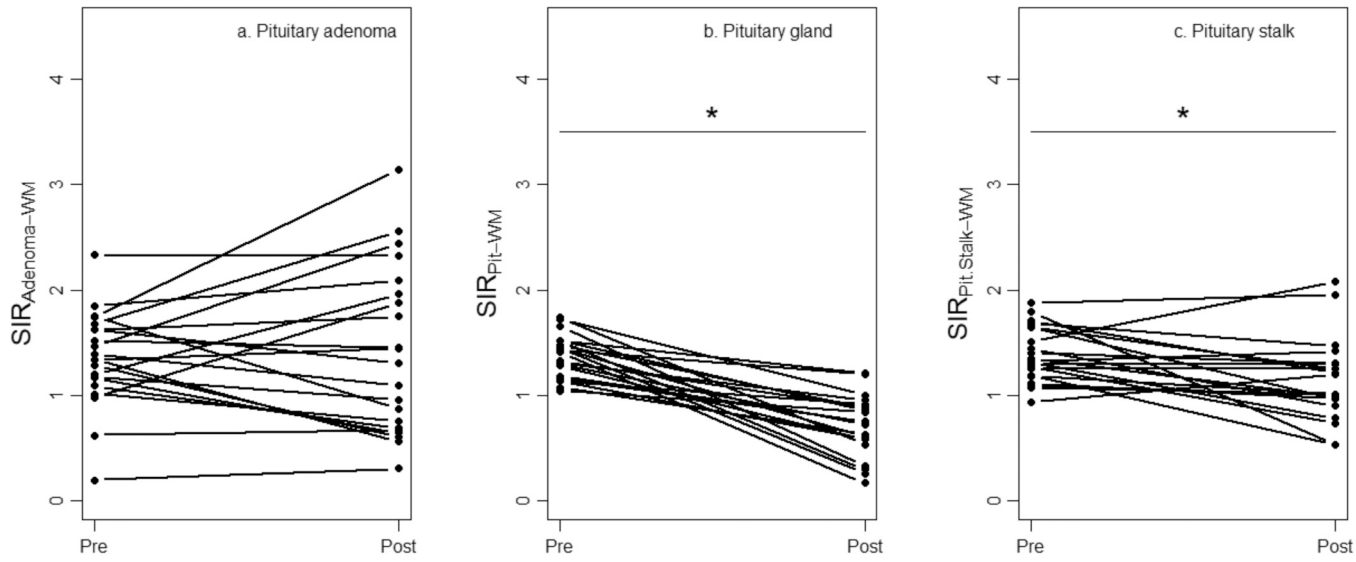

Fig. 5. Objective comparison of signal intensity ratio (SIR) between pre- and post-contrast 3D STIR FLAIR imaging. The pituitary adenoma (a) showed no significant difference in SIR between post-contrast 3D STIR FLAIR imaging and pre-contrast 3D STIR FLAIR imaging, although the tumor tended to show higher signal on post-contrast imaging compared with pre-contrast imaging. The pituitary gland (b) and stalk (c) demonstrated decreased SIR on post-contrast 3D STIR FLAIR imaging, although the stalk showed some trends with higher SI compared with the gland.

enhancements [27].

2D STIR FLAIR sequence is a 2D double inversion recovery variant with null signals from fat and water. One previous report used this sequence for the evaluation of optic neuritis and showed that CSF flow artifact, which had high signal intensities in the CSF around the optic nerves, posed a diagnostic problem [8]. We also noticed that this artifact affected image interpretation of the pituitary gland and optic nerves more seriously on 2D STIR FLAIR imaging than on 3D STIR FLAIR imaging (data not shown). 3D STIR FLAIR sequence is a variant of 3D TSE-based double inversion recovery sequences and has the following potential advantages over 2D STIR FLAIR sequence: higher spatial resolution, acquisition of isotropic 3D data set to reconstruct images in arbitrary directions, and reduced CSF flow artifacts. In the present study, pituitary adenomas tended to show higher signal on post-contrast 3D STIR FLAIR imaging compared with pre-contrast imaging, while all of the pituitary glands had a lower signal on post-contrast 3D STIR FLAIR imaging compared with pre-contrast imaging, resulting in increased contrast between the adenoma and the gland.

For the side-by-side comparison, 3D STIR FLAIR imaging showed the border between the adenoma and the pituitary gland more clearly compared with conventional 2D T1W imaging. This result may be explained mainly by the increased contrast between the adenoma and pituitary gland on 3D STIR FLAIR imaging for the following reasons: 1) decreased signal of the pituitary gland and 2) relatively high signal of the adenomas. For the first reason, decreased signal of the pituitary gland was observed on 3D STIR FLAIR imaging after contrast injection in all cases. Conventional post-contrast T1W imaging demonstrated increased contrast enhancement in the pituitary gland compared with other brain parenchyma because this tissue is not covered by the BBB. In contrast, on post-contrast 3D STIR FLAIR imaging, the T1 value of the pituitary gland can reach the null point on the STIR sequence because of the T1-shortening effect of gadolinium, resulting in suppression of the pituitary gland.

As for the second reason, the interpretation of SI in the adenomas on post-contrast 3D STIR FLAIR imaging was complex and was probably affected by several factors such as imaging sequences, lesion characteristics, and gadolinium concentrations. Post-contrast T1W imaging usually demonstrates pituitary adenomas with decreased contrast enhancement compared to the pituitary gland. In contrast, on post-contrast FLAIR imaging, Kubota et al. described that contrast enhancement of pituitary adenoma varied from hypo-, iso-, and hyperintensity compared with post-contrast T1W imaging [20]. These researchers indicated a close relationship between T2W SI in brain tumors and FLAIR enhancement. Chatain et al. reported that some pituitary microadenomas showed hyperintensity on post-contrast FLAIR imaging with negative findings on 3D GRE T1W imaging [22]. Azuma et al. indicated that cystic pituitary adenomas demonstrated cyst wall enhancement more widely than Rathke cleft cysts on post-contrast 3D FLAIR imaging, while the anterior lobe of the pituitary gland was not enhanced [27]. In our study, the relatively high signal of the adenomas may have been caused by post-contrast T1 relaxation time far from that of fat. Three cases (14%) exhibited donut-like enhancement along the inner margin of the tumor on 3D STIR FLAIR imaging, but not on 2D T1W imaging. Azuma et al. reported this enhancement was observed in 50% of cases with cystic pituitary adenomas on contrast-enhanced 3D FLAIR images and considered it a potential characteristic sign of cystic pituitary adenomas [27]. Therefore, 3D STIR FLAIR imaging can be useful for the qualitative diagnosis of pituitary lesions.

Identification of the pituitary stalk is crucial for the surgery of pituitary lesions to reduce the risk of postoperative diabetes insipidus. In our study, the pituitary stalk showed decreased SIR on post-contrast 3D STIR FLAIR imaging than pre-contrast imaging like the pituitary gland, although the stalk demonstrated some trends with higher SI compared with the gland. Thus, the pituitary stalk was visualized more clearly than the gland. Like the pituitary gland, the pituitary stalk lacks the BBB, and can enhance intensely on T1W imaging. Therefore, SIR of the stalk was decreased on post-contrast 3D STIR FLAIR imaging than pre-contrast imaging probably because of T1-shortening effect of gadolinium on STIR signal. The pituitary stalk showed a relatively intense enhancement on post-contrast FLAIR imaging, while the pituitary gland was mildly enhanced [28]. However, unlike contrast-enhanced T1W imaging, FLAIR enhancement in the pituitary gland can be difficult to recognize or show subtle changes due to intrinsic T2 prolongation on pre-contrast FLAIR imaging [28]. Azuma et al. also reported that the pituitary stalk had contrast enhancement on 3D FLAIR imaging, while the anterior lobe of the pituitary gland was often unenhanced, probably caused by T2 shortening due to a high gadolinium concentration or the sequence's sensitivity to the flow in the hypophyseal portal system [29]. Thus, the signal difference between the pituitary stalk and the gland on post-contrast 3D STIR FLAIR imaging may reflect different tissue

properties.

Our results show that 3D STIR FLAIR imaging is superior to 2D T1W imaging in depicting the intracavernous segment of the cranial nerves, as well as the optic nerves and chiasm. Contrast-enhanced 3D STIR imaging has been used for MR neurography, offering improved visualization of peripheral nerves by vascular and background suppression of the nerves, as mentioned above. In the present study, improved visualization of the intracavernous segment of the cranial nerves may be caused by a decreased signal of the cavernous sinus compared to the cranial nerves. The cavernous sinus is a venous space that is slow-flowing compared to the internal carotid artery. The internal carotid artery typically shows flow void because of the high flow on post-contrast SE T1W imaging, while the cavernous sinus exhibits contrast enhancement due to slow flow. On pre-contrast 3D STIR FLAIR imaging, the cavernous sinus demonstrated hyperintensity due to slow flow, which does not generate a flow void effect, in addition to shorter T2 values of its blood than those of CSF. In contrast, on post-contrast 3D STIR FLAIR imaging, the cavernous sinus showed a decreased signal because the T1 relaxation time of blood in vessels will be reduced after contrast agent administration [14]; therefore, the cavernous sinus reached the null point of fat on 3D STIR FLAIR imaging. In fact, previous reports demonstrated that venous signals were decreased on post-contrast 3D STIR imaging [14], which may support these constellations. This effect can facilitate the visualization of the cranial nerves in the cavernous sinus. However, 14% (3/21) of the cases in the present study showed partial hyperintensity of the cavernous sinus on post-contrast 3D STIR FLAIR imaging, predominantly in the medial venous compartment (Fig. 4). This phenomenon occurred because the T1 relaxation time of the cavernous sinus was far from that of fat, resulting in incomplete suppression of the sinus on post-contrast 3D STIR FLAIR imaging. Although the exact mechanism remains unclear, it may depend on various flow or gadolinium concentrations within different parts of the cavernous sinus based on anatomical variations [30]. On the other hand, improved visualization of the optic nerves and chiasm may be achieved by increased contrast between the nerves and CSF, in addition to reduced CSF flow artifacts. The depiction of these cranial nerves is helpful for diagnosing cranial neuropathies with morphological and signal changes by compression of pituitary lesions, as well as for planning a surgical approach.

There are several limitations to our study. First, our study is a retrospective evaluation of a limited number of patients. Second, some adenomas were diagnosed radiologically and clinically. Therefore, the risk of false-positive or false-negative diagnoses could not be excluded in the absence of pathological confirmation. False positives may result from technical artifacts or low image clarity. False negatives can occur if the SI in the adenomas is decreased, similar to the pituitary gland or cavernous sinus, which makes it difficult to distinguish between lesions and adjacent tissues. Third, the radiologic diagnosis of cavernous sinus invasion by pituitary adenoma is made based on the relationship between tumors and the internal carotid artery. Identification of the internal carotid artery is essential for evaluating cavernous sinus invasion. Post-contrast 3D STIR FLAIR imaging alone may fail to localize the internal carotid artery because its flow void can obscure interfaces between this artery and adjacent tissues, and may require pre-contrast 3D STIR FLAIR imaging.

5. Conclusion

3D STIR FLAIR imaging improved overall lesion conspicuity compared to conventional 2D T1W imaging. We suggest that 3D STIR FLAIR imaging is recommended as a supplemental technique when pituitary adenomas are invisible or equivocal on conventional imaging.

Ethical approval

All procedures performed in studies involving human participants were in accordance with the ethical standards of the institutional and/or national research committee and with the 1964 Helsinki declaration and its later amendments or comparable ethical standards.

Informed consent

This retrospective study was conducted at a single institution and approved by the Institutional Review Board of our institution. We obtained written informed consent for the procedures and opt-out consent for the use of retrospective clinical data from all patients.

Funding

This research did not receive any specific grant from funding agencies in the public, commercial, or not-for-profit sectors.

CRediT authorship contribution statement

Shimizu Hirokazu: Data curation, Writing – review & editing. **Nagawa Keita:** Formal analysis, Writing – review & editing. **Hara Yuki:** Formal analysis, Writing – review & editing. **Kozawa Eito:** Supervision, Writing – review & editing. **Tanaka Sayuri:** Data curation, Writing – review & editing. **Osawa Iichiro:** Conceptualization, Data curation, Formal analysis, Methodology, Writing – original draft.

Declaration of Competing Interest

The authors declare that they have no conflict of interest.

Acknowledgments

We gratefully thank Mr. Takashi Namiki and Mr. Masami Yoneyama of Philips Healthcare for technical assistance with this study.

References

[1] W.S. Bartynski, L. Lin, Dynamic and conventional spin-echo MR of pituitary microlesions, AJNR Am. J. Neuroradiol. 18 (1997) 965–972.
[2] M. Kinoshita, H. Tanaka, H. Arita, Y. Goto, S. Oshino, Y. Watanabe, T. Yoshimine, Y. Saitoh, Pituitary-targeted dynamic contrast-enhanced multisection CT for detecting MR imaging-occult functional pituitary microadenoma, AJNR Am. J. Neuroradiol. 36 (2015) 904–908.
[3] N. Patronas, N. Bulakbasi, C.A. Stratakis, A. Lafferty, E.H. Oldfield, J. Doppman, L. K. Nieman, Spoiled gradient recalled acquisition in the steady state technique is superior to conventional postcontrast spin echo technique for magnetic resonance imaging detection of adrenocorticotropin-secreting pituitary tumors, J. Clin. Endocrinol. Metab. 88 (2003) 1565–1569.
[4] S. Kakite, S. Fujii, M. Kurosaki, Y. Kanasaki, E. Matsusue, T. Kaminou, T. Ogawa, Three-dimensional gradient echo versus spin echo sequence in contrast-enhanced imaging of the pituitary gland at 3T, Eur. J. Radio. 79 (2011) 108–112.
[5] T. Sartoretti, E. Sartoretti, M. Wyss, Á. Schwenk, L. van Smoorenburg, B. Eichenberger, A. Najafi, C. Binkert, A.S. Becker, S. Sartoretti-Schefer, Compressed SENSE accelerated 3D T1w black blood turbo spin echo versus 2D T1w turbo spin echo sequence in pituitary magnetic resonance imaging, Eur. J. Radio. 120 (2019), 108667.
[6] R.J. Lien, I. Corcuera-Solano, P.S. Pawha, T.P. Naidich, L.N. Tanenbaum, Three-Tesla imaging of the pituitary and parasellar region: T1-weighted 3-dimensional fast spin echo cube outperforms conventional 2-dimensional magnetic resonance imaging, J. Comput. Assist Tomogr. 39 (2015) 329–333.
[7] J. Wang, Y. Wu, Z. Yao, Z. Yang, Assessment of pituitary micro-lesions using 3D sampling perfection with application-optimized contrasts using different flip-angle evolutions, Neuroradiology 56 (2014) 1047–1053.
[8] J. Hodel, O. Outteryck, A.L. Bocher, H. Zéphir, O. Lambert, M.A. Benadjaoud, D. Chechin, J.P. Pruvo, P. Vermersch, X. Leclerc, Comparison of 3D double inversion recovery and 2D STIR FLAIR MR sequences for the imaging of optic neuritis: pilot study, Eur. Radio. 24 (2014) 3069–3075.
[9] K.L. Gwet, Computing inter-rater reliability and its variance in the presence of high agreement, Br. J. Math. Stat. Psychol. 61 (2008) 29–48.
[10] J.R. Landis, G.G. Koch, The measurement of observer agreement for categorical data, Biometrics 33 (1977) 159–174.
[11] Y. Miki, M. Matsuo, S. Nishizawa, Y. Kuroda, A. Keyaki, Y. Makita, J. Kawamura, Pituitary adenomas and normal pituitary tissue: enhancement patterns on gadopentetate-enhanced MR imaging, Radiology 177 (1990) 35–38.
[12] M. Azuma, Z.A. Khant, M. Kitajima, H. Uetani, T. Watanabe, K. Yokogami, H. Takeshima, T. Hirai, Usefulness of contrast-enhanced 3D-FLAIR MR imaging for

differentiating rathke cleft cyst from cystic craniopharyngioma, AJNR Am. J. Neuroradiol. 41 (2020) 106–110.
[13] H.B. Lee, S.T. Kim, H.J. Kim, K.H. Kim, P. Jeon, H.S. Byun, J.W. Choi, Usefulness of the dynamic gadolinium-enhanced magnetic resonance imaging with simultaneous acquisition of coronal and sagittal planes for detection of pituitary microadenomas, Eur. Radio. 22 (2012) 514–518.
[14] W.C. Chen, Y.H. Tsai, H.H. Weng, S.C. Wang, H.L. Liu, S.L. Peng, C.F. Chen, Value of enhancement technique in 3D-T2-STIR images of the brachial plexus, J. Comput. Assist Tomogr. 38 (2014) 335–339.
[15] W. Wu, F. Wu, D. Liu, C. Zheng, X. Kong, S. Shu, D. Li, X. Kong, L. Wang, Visualization of the morphology and pathology of the peripheral branches of the cranial nerves using three-dimensional high-resolution high-contrast magnetic resonance neurography, Eur. J. Radio. 132 (2020), 109137.
[16] T. Zhang, Z. Xu, J. Chen, Z. Liu, T. Wang, Y. Hu, L. Shen, F. Xue, A. Novel, Approach for Imaging of Thoracic Outlet Syndrome Using Contrast-Enhanced Magnetic Resonance Angiography (CE-MRA), Short Inversion Time Inversion Recovery Sampling Perfection with Application-Optimized Contrasts Using Different Flip Angle Evolutions (T2-STIR-SPACE), and Volumetric Interpolated Breath-Hold Examination (VIBE), Med Sci. Monit. 25 (2019) 7617–7623.
[17] S. Naganawa, The technical and clinical features of 3D-FLAIR in neuroimaging, Magn. Reson Med Sci. 14 (2015) 93–106.
[18] I. Osawa, E. Kozawa, Y. Yamamoto, S. Tanaka, T. Shiratori, A. Kaizu, K. Inoue, M. Niitsu, Contrast enhancement of the normal infundibular recess using heavily T2-weighted 3D FLAIR, Magn. Reson Med Sci. (2021).
[19] I. Osawa, E. Kozawa, S. Tanaka, A. Kaizu, K. Inoue, T. Ikezono, T. Fujimaki, M. Niitsu, Signal and morphological changes in the endolymph of patients with vestibular schwannoma on non-contrast 3D FLAIR at 3 Tesla, BMC Med Imaging 21 (2021) 135.
[20] T. Kubota, K. Yamada, O. Kizu, T. Hirota, H. Ito, K. Ishihara, T. Nishimura, Relationship between contrast enhancement on fluid-attenuated inversion recovery MR sequences and signal intensity on T2-weighted MR images: visual evaluation of brain tumors, J. Magn. Reson Imaging 21 (2005) 694–700.
[21] G.U. Mehta, B.K. Montgomery, P. Raghavan, S. Sharma, L.K. Nieman, N. Patronas, E.H. Oldfield, P. Chittiboina, Different imaging characteristics of concurrent pituitary adenomas in a patient with Cushing's disease, J. Clin. Neurosci. 22 (2015) 891–894.
[22] G.P. Chatain, N. Patronas, J.G. Smirniotopoulos, M. Piazza, S. Benzo, A. Ray-Chaudhury, S. Sharma, M. Lodish, L. Nieman, C.A. Stratakis, P. Chittiboina, Potential utility of FLAIR in MRI-negative Cushing's disease, J. Neurosurg. 129 (2018) 620–628.
[23] H. Nakazawa, Y. Shibamoto, T. Tsugawa, Y. Mori, M. Nishio, T. Takami, M. Komori, C. Hashizume, T. Kobayashi, Efficacy of magnetic resonance imaging at 3 T compared with 1.5 T in small pituitary tumors for stereotactic radiosurgery planning, Jpn J. Radio. 32 (2014) 22–29.
[24] S. Naganawa, T. Koshikawa, T. Nakamura, H. Kawai, H. Fukatsu, T. Ishigaki, T. Komada, K. Maruyama, O. Takizawa, Comparison of flow artifacts between 2D-FLAIR and 3D-FLAIR sequences at 3 T, Eur. Radio. 14 (2004) 1901–1908.
[25] D.F. Kallmes, F.K. Hui, J.P. Mugler 3rd, Suppression of cerebrospinal fluid and blood flow artifacts in FLAIR MR imaging with a single-slab three-dimensional pulse sequence: initial experience, Radiology 221 (2001) 251–255.
[26] I. Osawa, E. Kozawa, T. Mitsufuji, T. Yamamoto, N. Araki, K. Inoue, M. Niitsu, Intravenous enhanced 3D FLAIR imaging to identify CSF leaks in spontaneous intracranial hypotension: Comparison with MR myelography, Eur. J. Radio. Open 8 (2021), 100352.
[27] M. Azuma, Z.A. Khant, Y. Kadota, G. Takeishi, T. Watanabe, K. Yokogami, H. Takeshima, T. Hirai, Added Value of Contrast-enhanced 3D-FLAIR MR Imaging for Differentiating Cystic Pituitary Adenoma from Rathke's Cleft Cyst, Magn. Reson Med Sci. 20 (2021) 404–409.
[28] E.K. Lee, E.J. Lee, S. Kim, Y.S. Lee, Importance of contrast-enhanced fluid-attenuated inversion recovery magnetic resonance imaging in various intracranial pathologic conditions, Korean J. Radio. 17 (2016) 127–141.
[29] M. Azuma, T. Hirai, Y. Kadota, Z.A. Khant, Y. Hattori, M. Kitajima, H. Uetani, Y. Yamashita, Circumventricular organs of human brain visualized on post-contrast 3D fluid-attenuated inversion recovery imaging, Neuroradiology 60 (2018) 583–590.
[30] S. Tanoue, M. Hirohata, Y. Takeuchi, K. Orito, S. Kajiwara, T. Abe, Venous anatomy of the cavernous sinus and relevant veins, J. Neuroendovasc. Ther. advpub (2020).